# Formation of nanocrystalline particles on the basis of La$_2$(Ni,Mn,Fe)$_2$O$_6$ variable composition phases having a structure of double perovskite under conditions of solution combustion

Denis D. Averkiev[1,2,a], Lyudmila L. Larina[3], Oleg I. Shevaleevskiy[3,b], Oksana V. Almjasheva[1,2,c]

[1]Ioffe Institute, St. Petersburg, Russia
[2]St. Petersburg State Electrotechnical University "LETI", St. Petersburg, Russia
[3]Solar Photovoltaic Laboratory, Emanuel Institute of Biochemical Physics, Moscow, Russia

[a]swnesli2019@gmail.com, [b]shevale2006@yahoo.com, [c]almjasheva@mail.ru

Corresponding author: Oksana V. Almjasheva, almjasheva@mail.ru

ABSTRACT Nanocrystalline particles on the basis of La$_2$(Ni,Mn,Fe)$_2$O$_6$ variable composition phases of a double perovskite structure have been produced by glycine-nitrate combustion. The size of crystallites grows from 5 to 45 nm with an increase in iron content of synthesized particles. It is demonstrated that iron unevenly builds into octahedral sites of nickel and manganese ions substituting mainly manganese ions. At the same time, the dependence of double perovskite unit cell volume on the iron ions concentration is well described by Retgers' law.

KEYWORDS double perovskite, nanocrystals, solution combustion, photovoltaics.

FOR CITATION Averkiev D.D., Larina L.L., Shevaleevskiy O.I., Almjasheva O.V. Formation of nanocrystalline particles on the basis of La**2**(Ni,Mn,Fe)**2**O**6** variable composition phases having a structure of double perovskite under conditions of solution combustion. *Nanosystems: Phys. Chem. Math.*, 2022, **13** (6), 655–661.

## 1. Introduction

Double perovskites of general formula $A_2BB'O_6$ with $d$-elements ions in octahedral sites ($B$, $B'$) are well known for their electronic, transport and magnetic properties [1–10]. In these compounds, cation sublattices of $d$-elements – $B$ and $B'$, as a rule, have the capability of ferromagnetic or antiferromagnetic ordering [11], which determines, to a great extent, the formation of physical properties of materials based on them. $B$ and $B'$ elements variation or their partial substitution for other elements may significantly affect the properties of materials [12–14]. Changing the properties by the partial substitution of ions in octahedral sublattices may also be defined by the peculiarities of the electronic structure of substituting cations and by their impact on the redistribution of major cations – $B$ and $B'$ – to octahedral sites, as, for example, in the case of phases having a chrysoberyl structure Be$MeMe'$O$_4$ described in [15].

Currently, La$_2$NiMnO$_6$ seems to be one of the most in-demand compounds with the double perovskite structure. The interest in this compound is due primarily to its high interrelated magnetic and electrophysical properties [16–24]. Owing to such range of properties, materials on the basis of La$_2$NiMnO$_6$ are considered as promising for the use in spintronics [16–18]. Furthermore, La$_2$NiMnO$_6$ has been extensively studied recently with regard to the use of this compound in photovoltaics [25–30].

In order to obtain La$_2$NiMnO$_6$, solid-phase synthesis is usually used. Depending on the conditions of the synthesis, La$_2$NiMnO$_6$ may be formed as three different crystal structures – rhombohedric (R-3c), monoclinic (P2$_1$/n) or orthorombic (Pbnm) [16, 19, 22, 31]. In [31], it is noted that exactly the temperature mode of the synthesis defines the formation of one or other structure. However, the analysis of findings from a great number of researches published by now [13, 16, 19, 22, 28, 31–35] does not allow tracing clear correlation of La$_2$NiMnO$_6$ structure with the temperature at which the compound was produced.

It is known that the temperature of the synthesis can greatly affect the extent of elements ordering during their distribution to various sites in crystals [36, 37]. The temperature impact is particularly significant for the redistribution of ions to various structural sites in cases where they take positions with similar values of coordination numbers [15, 38]. However, it is far from being the only factor defining the distribution of ions by sites [39–43]. Papers [42, 43] have shown that the ordering of $d$-element cations in octahedral sites depends on the La$_2$NiMnO$_6$ production method. There are

also discrepancies in respect of the impact of synthesis conditions on the oxidation rate of nickel and manganese ions in $La_2NiMnO_6$ compound and, therefore, on the properties of double perovskite [21, 22, 35, 44–46].

A profound effect on properties of materials may be exerted by the size of particles and crystallites of phases that form them, especially with the transition into nano-scale range of their values [47–53]. It should be noted that, as shown in [31–35, 42–46, 50, 51, 54], the influence of synthesis methods and conditions on properties is specifically great for nanocrystalline materials. In this regard, a typical example is the effect of crystallite sizes and conditions of synthesis of $BiFeO_3$ nano-powders on their magnetic properties [50].

One of the promising methods of synthesis of complex oxides is the method of glycine-nitrate combustion [50–65]. At the same time, this method not always guarantees the possibility of one-stage synthesis of complex oxide phases [22, 28, 32, 33, 46, 58]. Another problem of producing the compounds by the glycine-nitrate combustion method is associated with the chance of evaporation in the combustion front under conditions of high temperatures of the most volatile ingredients of the synthesized phases and, therefore, disturbance of stoichiometry of the compounds produced. It is also difficult to adjust the size of crystallites of forming phases when using this method.

The above-listed considerations initiated the research in $La_2(Ni,Mn,Fe)_2O_6$ peculiarities of variable composition nanocrystalline double perovskite formation under conditions of glycine-nitrate combustion and the analysis of the impact of iron nitrate introduction into source reagents on the composition, structural parameters and crystallite size of the synthesized complex oxide phase.

## 2. Experimental

The synthesis of $La_2(Ni,Mn,Fe)_2O_6$ variable composition nanocrystalline phase, in which the iron content, according to the given formula, varies from 0 to 1, was performed by glycine-nitrate combustion in accordance with the procedure described in detail in [65]. Water solution containing manganese (II) sulphate, lanthanum nitrate, nickel (II) nitrate and iron (III) nitrate in accordance with the set ratio of cations in the synthesized phase, were mixed with glycine in the proportion complying with the stoichiometry of the glycine-nitrate combustion reaction. The mixture was brought to the boil. Once most of the water has evaporated, a gel-like mixture was produced, which self-ignited and burnt generating a porous powder product.

The nominal iron content introduced into the system was calculated on the assumption of even substitution of $d$-element atoms in octahedral sites of nickel and manganese – $La_2Ni_{1-x}Fe_xMn_{1-x}Fe_xO_6$, where $x$ value varied in the range of 0–1 at 0.2 intervals.

The elemental composition of the materials obtained was determined by the X-ray fluorescence analysis (XRF) using Spectroscan GF-2 device.

The study of sample phase composition was performed by X-ray powder diffraction by means of Rigaku SmartLab 3 diffractometer ($CuK_\alpha$). The identification of peaks in the diffraction pattern was performed using PDWin 4.0 software suite and Crystallographica Search-Match package. The average size of crystallites was calculated on the basis of data on X-ray diffraction line profile broadening using Scherrer equation and a software package (SmartLabStudio III).

The morphology of the produced materials was determined by means of scanning electron microscopy (Vega3 Tescan microscope).

## 3. Findings and discussions

A powder material the morphology of which changed with an increase in iron amount in the system was obtained by the glycine-nitrate combustion method (Fig. 1). For an iron-free sample, it is typical to have a sponge-like structure (Fig. 1). In iron-containing samples, the structure of particles with interpenetrating solid phase and pores is consistently changing with an increase in iron content of the reaction system. At a nominal value of $x = 0.2$ in $La_2Ni_{1-x}Fe_xMn_{1-x}Fe_xO_6$ synthesized phase, pores of sizes varying from 0.3 to 2.0 microns are observed in photomicrographs of particles. At $x = 0.4$, the pore size falls in the range of 0.5–2.5 microns. At $x = 0.6$, the pore size varies generally in the range of 0.5–5 microns. A further increase in the nominal values of $x$ in $La_2Ni_{1-x}Fe_xMn_{1-x}Fe_xO_6$ synthesized double perovskite to $x = 0.8$ leads to a decrease in both the pore quantity and the minimum size, and at $x = 1$, the sample comprises solid aggregates consisting of almost pore-free plate-like particles.

Elemental composition of the materials produced presented in Table 1 shows significant differences in the nominal and actual compositions of synthesized phases of $La_2(Ni,Mn,Fe)_2O_6$ containing all the three elements in octahedral sites. As distinct from these cases, the nominal and actual compositions of $La_2NiMnO_6$ double perovskite and $LaFeO_3$ lanthanum ferrite having the perovskite structure are practically identical. The analysis of the data given in Table 1 shows that iron ions chiefly substitute manganese ions in their octahedral sites. This may be related with the fact that in the process of glycine-nitrate combustion in the combustion wave at high temperatures and low values of gas atmosphere oxygen potential, manganese ions exist mainly in the state of $Mn^{3+}$ oxidation [67], and at the moment of entry into the structure of double perovskite, due to the proximity of $Mn^{3+}$ and $Fe^{3+}$ ionic radius values [68], manganese ions are substituted for iron with ease. It should be noted that in such case, owing to the local charge neutralization effect [69], one can expect nickel stabilization in the state of Ni (III) in $La_2(Ni,Mn,Fe)_2O_6$ double perovskite. In publications, the chance of finding $Ni^{3+}$ and $Mn^{3+}$ ions in double perovskite in octahedral sites was mentioned in [21, 22, 44]. A significantly greater

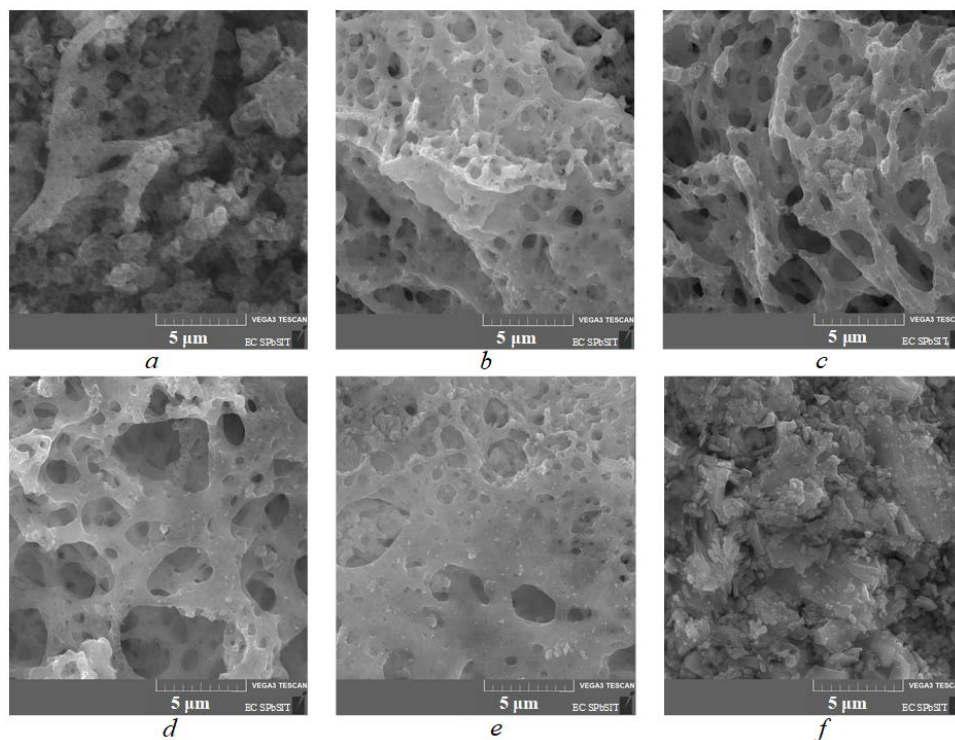FIG. 1. Photomicrographs of samples with nominal composition of La$_2$Ni$_{1-x}$Fe$_x$Mn$_{1-x}$Fe$_x$O$_6$. $a - x = 0$; $b - x = 0.2$; $c - x = 0.4$; $d - x = 0.6$; $e - x = 0.8$; $f - x = 1$

TABLE 1. Elemental composition of samples with regard to distribution of $d$-elements over octahedral sites

| Nominal composition of samples La$_2$Ni$_{1-x}$Fe$_x$Mn$_{1-x}$Fe$_x$O$_6$ | Sample composition according to X-ray fluorescence analysis | | | | | | |
|---|---|---|---|---|---|---|---|
| | Recalculation to the double perovskite formula La$_2$Ni$_{1-x}$Fe$_x$Mn$_{1-y}$Fe$_y$O$_6$ | | | | | | Total |
| $x(2x)$Fe | La | $(1-x)$Ni | $x$Fe | $(1-y)$Mn | $y$Fe | $(x+y)$Fe | Fe |
| 0.0 (0.0) | 2 | 1.00 | 0.00 | 1.00 | 0.00 | 0.00 | 0.00 |
| 0.2 (0.4) | 2 | 1.00 | 0.00 | 0.74 | 0.26 | 0.26 | 0.43 |
| 0.4 (0.8) | 2 | 0.79 | 0.21 | 0.43 | 0.57 | 0.78 | 0.88 |
| 0.6 (1.2) | 2 | 0.59 | 0.41 | 0.31 | 0.69 | 1.10 | 1.47 |
| 0.8 (1.6) | 2 | 0.28 | 0.72 | 0.15 | 0.85 | 1.57 | 1.81 |
| 1.0 (2.0) | 2 | 0.00 | 1.00 | 0.00 | 1.00 | 2.00 | 2.00 |

difference in ionic radii of Ni$^{3+}$ and Fe$^{3+}$ as compared to Mn$^{3+}$ and Fe$^{3+}$ in this case, apparently, is the main cause of the predominant substitution of manganese ion octahedral sites for iron ions. It should be noted that the result obtained contradicts to some extent to the conclusion made in [13,14] where the authors concluded that doping La$_2$NiMnO$_6$ double perovskite with $d$-elements takes place as a result of Ni substitution in octahedral sites. The explanation of this discrepancy may be the fact that in the given papers the substitution of ions in octahedral sites of La$_2$NiMnO$_6$ double perovskite was performed by other methods and for other $d$-elements.

As shown by the analysis of the data given in Table 1, the fraction of iron required for substitution of nickel and manganese in octahedral sites of double perovskite is less than the total iron content of the sample. This can be associated with both the non-stoichiometry of double perovskite, the possibility of which it was noted in [23], and with the localization of a part of iron-containing component in the non-autonomous (intergranular) phase, which occurs especially frequently in nanocrystalline materials [70–74].

According to the X-ray diffractometry data (Fig. 2), iron-containing samples are single-phase and comprise double perovskite having an orthorhombic structure. In case of complete substitution of nickel and manganese ions in double

perovskite for iron, peaks corresponding to the phase of $LaFeO_3$ (card 37-1493) and having the structure of perovskite with an orthorhombic crystal lattice are recorded in the X-ray diffractogram. Low-intensity reflexes corresponding to the phases of $La_2NiO_4$ and $MnO_2$ (Fig. 2), which are missing in all other samples containing iron even in small amounts, are recorded in the X-ray diffractogram of an iron-free sample. This may be associated with a higher temperature in the glycine-nitrate combustion front in the presence of iron oxide being a glycine oxidation catalyst, which was also noted in some other papers on glycine-nitrate synthesis of iron-containing oxide phases [57, 58, 65, 66]. The increase in temperature of the synthesis, in turn, intensifies the double perovskite formation process. The assumption that, during the synthesis of double perovskite with the composition $La_2NiMnO_6$, the temperature in the combustion front is insufficient to fully complete the process of the target product formation may be confirmed by the fact that, according to the data of papers [28, 32, 33, 46], the authors carried out additional heat treatment of combustion products. Another indirect proof of more intense running of the glycine-nitrate synthesis of double perovskite as its composition includes iron oxide is an increase in the size of crystallites of $La_2(Ni,Mn,Fe)_2O_6$ variable composition phase with an increasing iron content of the phase (Fig. 3).
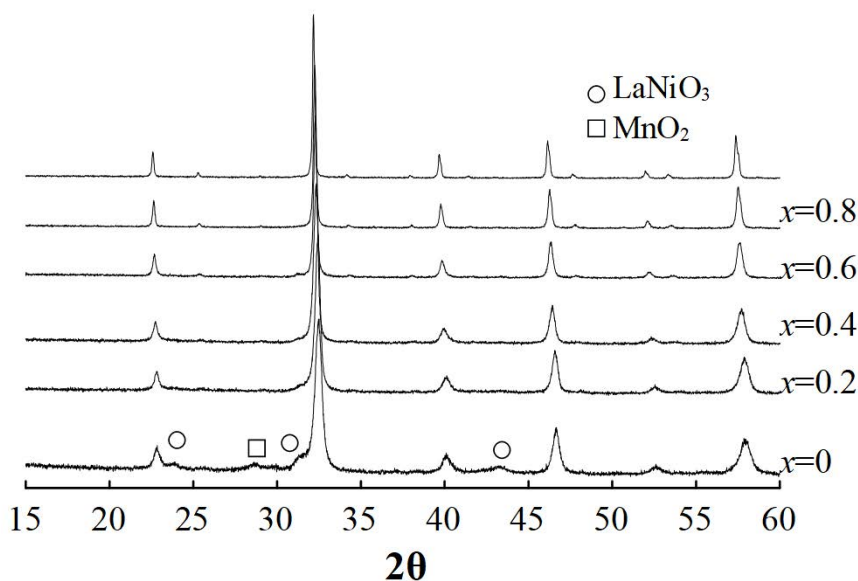


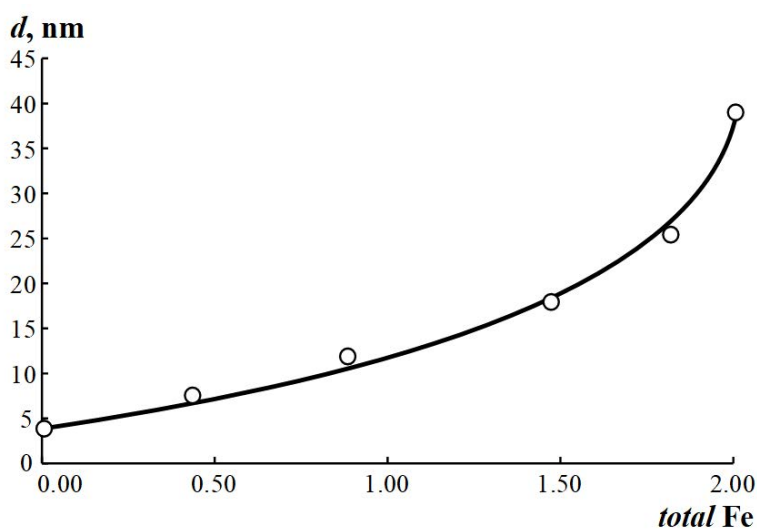FIG. 2. X-ray diffractograms of samples produced by the glycine-nitrate combustion method



FIG. 3. Sizes of phase $La_2(Ni,Mn,Fe)_2O_6$ crystallites versus actual total iron content of the system (Table 1)

A higher iron content of the samples leads to the displacement of reflexes to the field of smaller angles, i.e., to an increase in unit cell parameters. The analysis of the character of dependence of the unit cell volume on the iron amount $- (x + y)$, in phase $La_2Ni_{1-x}Fe_xMn_{1-y}Fe_yO_6$, according to the data of Table 1 (Fig. 4), testifies that this dependence

complies with Retgers' law. Comparison of the data on the dependence of double perovskite unit cell volume on its $Fe^{3+}$ ions content with the data on ionic radii of $Ni^{2+}$, $Ni^{3+}$, $Mn^{3+}$, $Mn^{4+}$ and $Fe^{3+}$ in octahedral coordination may serve as an indirect proof that iron ions entering the structure of double perovskite facilitate stabilization of Ni and Mn cations in charge states of $Ni^{3+}$ and $Mn^{3+}$ since exactly in this case an increase in double perovskite unit cell volume in accordance with the dependence shown in Fig. 4 may be expected.
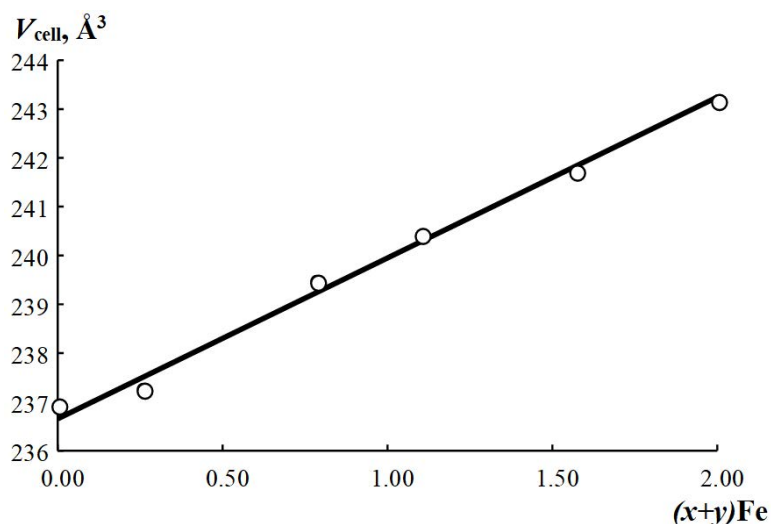


FIG. 4. Dependence of La$_2$(Ni$_{1-x}$Fe$_x$)(Mn$_{1-y}$Fe$_y$)O$_6$ unit cell volume on the amount of iron in the system (iron amount is given according to the data of Table 1)

## 4. Conclusion

Thus, it may be concluded that La$_2$(Ni,Mn,Fe)O$_6$ nanocrystalline phases of variable composition on the basis of double perovskite with an orthorhombic structure can be obtained by the glycine-nitrate combustion method without any additional heat treatment. Iron ions predominantly occupy octahedral sites of manganese and stabilize nickel and manganese in the states $Ni^{3+}$, $Mn^{3+}$. The size of crystallites in the formed phases grows from 5 to 45 nm with an increase in iron amount in the system.

## References

[1] Blasse G. Ferromagnetic interactions in non-metallic perovskites. *J. Phys. Chem. Solids*, 1965, **26**, P. 1969–1971.

[2] Goodenough J.B., Wold A., Arnott R.J., Menyuk N. Relationship between crystal symmetry and magnetic properties of ionic compounds containing $Mn^{3+}$. *Phys. Rev.*, 1961, **124**, P. 373–384.

[3] Kojima A., Teshima K., Shirai Y., Miyasaka T. Organometal halide perovskites as visible-light sensitizers for photovoltaic cells. *J. Am. Chem. Soc.*, 2009, **131**(17), P. 6050–651.

[4] Grinberg I., West D.V., Torres M., Gou G., Stein D.M., Wu L., Chen C., Gallo E.M., Akbashev A.R., Davies P.K., Spanier J.E., Rappe A.M. Perovskite oxides for visiblelight-absorbing ferroelectric and photovoltaic materials. *Nature*, 2013, **503**, P. 509–512.

[5] Wang F., Grinberg I., Rappe A.M. Semiconducting ferroelectric photovoltaics through $Zn^{2+}$ doping into KNbO$_3$ and polarization rotation. *Phys. Rev.*, 2014, **89**(23), P. 235105.

[6] Nechache R., Harnagea C., Li S., Cardenas L., Huang W., Chakrabartty J., Rosei F. Bandgap tuning of multiservice oxide solar cells. *Nat. Photonics*, 2015, **9**, P. 61–67.

[7] Liu Y.P., Chen S.H., Tung J.C., Wang Y.K. Investigation of possible half-metal material on double perovskites Sr$_2$BBO$_6$ (B, B=3d transition metal) using firstprinciple calculations. *Solid State Commun.*, 2012, **152**(11), P. 968–973.

[8] Berger R.F., Neaton J.B. Computational design of low-band-gap double perovskites. *Physical Review B*, 2012, **86**(16), P. 165211.

[9] Troullier N., Martins J.L. Efficient Pseudopotentials for plane wave calculations. *Physical Review B*, 1991, **43**(3), P. 1993–2006.

[10] Giannozzi P., Baroni S., Bonini N. Quantum Espresso: a modular and open-source software project for quantum simulations of materials. *J. Phys. Condens. Matter.*, 2009, **21**, P. 395502.

[11] Kobayashi K.I., Kimura T., Sawada H., Terakura K., Tokura Y. Room-temperature magnetoresistance in an oxide material with an ordered double-perovskite structure. *Nature*, 1998, **395**, P. 677–680.

[12] Najar F.A., Abass S., Sultan K., Kharadi M. A., Malik G.F.A., Samad R. Comparative study of optical properties of substitutionally doped La$_2$NiMnO$_6$ double perovskite ceramic: A potential candidate for solar cells and dielectrics. *Physica B: Condensed Matter*, 2021, **621**, P. 413311.

[13] Tirmali P.M., Mane S.M., Kadam S.L., Kulkarni S.B. Effect of substitutions on dielectric behavior of La$_2$NiMnO$_6$. *Chinese Journal of Physics*, 2018, **56**(2), P. 525–537.

[14] Gan H., Wang C., Shen Q. Improved magnetic performance of Co-doped La$_2$NiMnO$_6$ ceramics prepared at low temperature. *Journal of the European Ceramic Society*, 2020, **40**(5), P. 1909–1916.

[15] Gusarov V.V., Matrosov V.N., Semin E.G., Suvorov S.A. Theoretical analysis of thermodynamic parameters of mixing during intracrystalline exchange in chrysoberyl. *Catalytic processes and catalysts*. LTI im. Lensovet, Leningrad, 1983, P. 76–81. In Russian

[16] Rogado N.S., Li J., Sleight A.W., Subramanian M.A. Magnetocapacitance and magnetoresistance near room temperature in a ferromagnetic semiconductor: $La_2NiMnO_6$. *Adv. Mater.*, 2005, **17**(18), P. 2225–2227.

[17] Spurgeon S.R., Du Y., Droubay T., Devaraj A., Sang X., Longo P., Yan P., Kotula P.G., Shutthanandan V., Bowden M.E., LeBeau J.M., Wang C., Sushko P.V., Chambers S.A. Competing pathways for nucleation of the double perovskite structure in the epitaxial synthesis of $La_2MnNiO_6$. *Chem. Mater.*, 2016, **28**(11), P. 3814–3822.

[18] Choudhury D., Mandal P., Mathieu R., Hazarika A., Rajan S., Sundaresan A., Waghmare U.V., Knut R., Karis O., Nordblad P., Sarma D.D. Near-room-temperature colossal magnetodielectricity and multiglass properties in partially disordered $La_2NiMnO_6$. *Phys. Rev. Lett.*, 2012, **108**(12), P. 127201.

[19] Iliev M.N., Guo H., Gupta A. Raman spectroscopy evidence of strong spin-phonon coupling in epitaxial thin films of the double perovskite $La_2NiMnO_6$. *Appl. Phys. Lett.*, 2007, **90**, P. 151914.

[20] Bull C.L., Gleeson D., Knight K.S. Determination of B-site ordering and structural transformations in the mixed transition metal perovskites $La_2CoMnO_6$ and $La_2NiMnO_6$. *J. Phys. Condens. Matter.*, 2003, **15**(29), P. 4927–4936.

[21] Joly V.L.J., Joy P.A., Date S.K., Gopinath C.S. Two ferromagnetic phases with different spin states of Mn and Ni in $LaMn_{0.5}Ni_{0.5}O_3$. *Phys. Rev. B.*, 2002, **65**(18), P. 184416.

[22] Dass R.I., Yan J.Q., Goodenough J.B. Oxygen stoichiometry, ferromagnetism, and transport properties of $La_{2-x}NiMnO_{6+\delta}$. *Phys. Rev. B.*, 2003, **68**(6), P. 64415.

[23] Chandrasekhar K.D., Das A.K., Mitra C., Venimadhav A. The extrinsic origin of the magnetodielectric effect in the double perovskite $La_2NiMnO_6$. *J. Phys. Condens. Matter.*, 2012, **24**(49), P. 495901.

[24] Blanco J., García J., Sanchez M.C., Campo J., Subías G., P'erez-Cacho J. Magnetic properties of $LaNi_{1-x}Mn_xO^{3+\delta}$ perovskites. *Eur. Phys. J. B.*, 2002, **30**, P. 469–479.

[25] Kozlov S.S., Alexeeva O.V., Nikolskaia A.B., Shevaleevskiy O.I., Averkiev D.D., Kozhuhovskaya P.V., Almjasheva O.V., Larina L.L. Double perovskite oxides $La_2NiMnO_6$ and $La_2Ni_{0.8}Fe_{0.2}MnO_6$ for inorganic perovskite solar cells. *Nanosystems: Phys. Chem. Math.*, 2022, **13**(3), P. 314–319.

[26] Nikolskaia A.B., Kozlov S.S., Karyagina O.K. Alexeeva O.V., Almjasheva O.V., Averkiev D.D., Kozhuhovskaya P.V., Shevaleevskiy O.I. Cation Doping of $La_2NiMnO_6$ complex oxide with the double perovskite structure for photovoltaic applications. *Russ. J. Inorg. Chem.*, 2022, **67**(6), P. 921–925.

[27] Nikolskaia A.B., Vildanova M.F., Kozlov S.S., Almjasheva O.V., Gusarov V.V., Shevaleevskiy O.I. High performance tandem perovskite-silicon solar cells with very large bandgap photoelectrodes. *Nanosystems: Phys. Chem. Math.*, 2021, **12**(2), P. 246–251.

[28] Lan C., Zhao S., Xu T., Ma J., Hayase S., Ma T. Investigation on structures, band gaps, and electronic structures of lead free $La2_2NiMnO_6$ double perovskite materials for potential application of solar cell. *J. Alloys Compd.*, 2016, **655**, P. 208–214.

[29] Dixit H., Punetha D., Pandey S.K. Improvement in performance of leadfree inverted perovskite solar cell by optimization of solar parameters. *Optik*, 2019, **179**, P. 969–976.

[30] Kumar M., Prajapati B., Raj A., Anshul A., Sati P.C., Sahni M., Kumar A. Progresses and challenges in the structural and magnetic properties of double perovskite $La_2NiMnO_6$ with their applications in solar energy. *Materials Today: Proceedings*, 2022, **49**(8), P. 3088–3092.

[31] de Azevedo Filho J.B., Souza R.F., Queiroz J.C.A., Costa T.H.C., Sena C.P.S., Fonseca S.G.C., da Silva A.O., Oliveira J.B.L. Theoretical and experimental investigation of the structural and magnetic properties of $La_2NiMnO_6$. *Journal of Magnetism and Magnetic Materials*, 2021, **527**, P. 167770.

[32] Nasir M., Kumar S., Patra N., Bhattacharya D., Jha S.N., Basaula D.R., Bhatt S., Khan M., Liu S.-W., Biring S., Sen S. Role of antisite disorder, rare-earth size, and superexchange angle on band gap, Curie temperature, and magnetization of $R_2NiMnO_6$ double perovskites. *ACS Appl. Electron. Mater.*, 2019, **1**(1), P. 141–153.

[33] Kumar M, Prajapati B., Singh A., Kumar S., Kumar A., Mittal S., Aditya. Structural, optical and magneto-electric coupling analysis in 'Y' doped double perovskite $La_2NiMnO_6$ nanoparticles. *Chemical Physics*, 2020, **532**, P. 110688.

[34] Gaikwad V.M., Yadav K.K., Lofland S.E., Ramanujachary K.V., Chakraverty S., Ganguli A.K., Jha M. New low temperature process for stabilization of nanostructured $La_2NiMnO_6$ and their magnetic properties. *Journal of Magnetism and Magnetic Materials*, 2019, **471**, P. 8–13.

[35] Singh M.P., Truong K.D., Jandl S., Fournier P. Long-range Ni/Mn structural order in epitaxial double perovskite $La_2NiMnO_6$ thin films. *Phys. Rev. B.*, 2009, **79**, P. 224421.

[36] Reznitsky L.A. *Solid state calorimetry (structural, magnetic, electronic transformations).* Moscow State University, Moscow, 1981, 184 p. In Russian

[37] Reznitsky L.A. *Chemical bonding and transformations of oxides.* Moscow State University, Moscow, 1991, 168 p. In Russian

[38] Gusarov V.V., Semin E.G. State diagram of the subsolidus region of the quasi-binary system $BeAl_2O_4–[BeFe_2O_4]$. *Rus. J. Inorg. Chem.*, 1992, **37**(9), P. 2092–2096. In Russian

[39] Reznitsky L.A. *Crystal energetics of oxides.* Dialog – Moscow State University, Moscow, 1998, 146 p. In Russian

[40] Krasilin A.A., Gusarov V.V. Redistribution of Mg and Ni cations in crystal lattice of conical nanotube with chrysotile structure. *Nanosystems: Phys., Chem., Math.*, 2017. **8**(5), P. 620–627.

[41] Saxena S.K. *Thermodynamics of rock-forming crystalline solutions.* Springer, Berlin, Heidelberg, 1973, 188 p.

[42] Sayed F.N., Achary S.N., Jayakumar O.D. Role of annealing conditions on the ferromagnetic and dielectric properties of $La_2NiMnO_6$. *J. Mater. Res.*, 2011, **26**, P. 567–577.

[43] Balcells L., Navarro J., Bibes M., Roig A., Mart*ı*nez B., Fontcuberta J. Cationic ordering control of magnetization in $Sr_2FeMoO_6$ double perovskite. *Appl. Phys. Lett.*, 2001, **78**, P. 781–783.

[44] Pal S., Sharada G., Goyal M., Mukherjee S., Pal B., Saha R., Sundaresan A., Jana S., Karis O., Freeland J.W., Sarma D.D. Effect of anti-site disorder on magnetism in $La_2NiMnO_6$, *Phys. Rev. B*, 2018, **97**, P. 165137.

[45] Wang X., Sui Y., Li Y., Li L., Zhang X., Wang Y., Liu Z., Su W., Tang J. The influence of the antiferromagnetic boundary on the magnetic property of $La_2NiMnO_6$. *Appl. Phys. Lett.*, 2009, **95**, P. 252502.

[46] Nasir M., Khan M., Kumar S., Bhatt S., Patra N., Bhattacharya D., Jha S.N., Biring S., Sen S. The effect of high temperature annealing on the antisite defects in ferromagnetic $La_2NiMnO_6$ double perovskite. *Journal of Magnetism and Magnetic Materials*, 2019, **483**, P. 114–123.

[47] Gusarov V.V., Ishutina Z.N., Malkov A.A., Malygin A.A. Peculiarities of the solid-phase chemical reaction in formation of mullite in the nanosize film composition. *Doklady Akademii Nauk*, 1997, **357**(2), P. 203–205. In Russian

[48] Fokin B.S., Belenkiy M.Ya., Almjashev V.I., Khabensky V.B., Almjasheva O.V., Gusarov V.V. Critical heat flux in a boiling aqueous dspersion of nanoparticles. *Tech. Phys. Lett.*, 2009, **35**(5), P. 440–442.

[49] Yudin V.E., Otaigbe J.U., Svetlichnyi V.M., Korytkova E.N., Almjasheva O.V., Gusarov V.V. Effects of nanofiller morphology and aspect ratio on the rheo-mechanical properties of polimide nanocomposites. *EXP. Pol. Lett.*, 2008, **2**(7), P. 485–493.

[50] Lomanova N.A., Panchuk V.V., Semenov V.G., Pleshakov I.V., Volkov M.P., Gusarov V.V. Bismuth orthoferrite nanocrystals: magnetic characteristics and size effects. *Ferroelectrics*, 2020, **569**, P. 240–250.

[51] Popkov V.I., Almjasheva O.V., Semenova A.S., Kellerman D.G., Nevedomskiy V.N., Gusarov V.V. Magnetic properties of YFeO$_3$ nanocrystals obtained by different soft-chemical methods. *Journal of Materials Science: Materials in Electronics*, 2017, **28**(10), P. 7163–7170.

[52] Prylypko, S.Y., Akimov, G.Y., Revenko, Y.F. et al. Crystallite size and magnetic properties of La$_{0.7}$Mn$_{1.3}$O$_{3\pm\Delta}$. *Tech. Phys.*, 2010, **55**(7), P. 1056–1057.

[53] Nag A., Bose R.S.C., Venu K.S., Singh H. Influence of particle size on magnetic and electromagnetic properties of hexaferrite synthesised by sol-gel auto combustion route. *Ceramics International*, 2022, **48**(11), P. 15303–15313.

[54] Proskurina O.V., Sokolova A.N., Sirotkin A.A., Abiev R.Sh., Gusarov V.V. Role of Hydroxide Precipitation Conditions in the Formation of Nanocrystalline BiFeO$_3$. *Russ. J. Inorg. Chem.*, 2021, **66**(2), P. 163–169.

[55] Rogachev A.S., Mukasyan A.S. *Combustion for the synthesis of materials: an introduction to structural macrokinetics*. FIZMATLIT, Moscow, 2013, 400 p.

[56] Ostroushko A.A., Russkikh O.V. Oxide material synthesis by combustion of organic-inorganic compositions. *Nanosystems: Phys., Chem., Math.*, 2017, **8**(4), P. 476–502.

[57] Komlev A.A., Gusarov V.V. Glycine-nitrate combustion synthesis of nonstoichiometric Mg-Fe spinel nanopowders. *Inorg Mater.*, 2014, **50**(12), P. 1247–1251.

[58] Popkov V.I., Almjasheva O.V., Schmidt M.P., Izotova S.G., Gusarov V.V. Features of nanosized YFeO$_3$ formation under heat treatment of glycine–nitrate combustion products. *Russ. J. Inorg. Chem.*, 2015, **60**(10), P. 1193–1198.

[59] Popkov V.I., Almjasheva O.V., Nevedomskyi V.N., Sokolov V.V., Gusarov V.V. Crystallization behavior and morphological features of YFeO$_3$ nanocrystallites obtained by glycine-nitrate combustion. *Nanosystems: Phys., Chem., Math.*, 2015, **6**(6), P. 866–874.

[60] Lomanova N.A., Tomkovich M.V., Sokolov V.V., Gusarov V.V. Special features of formation of nanocrystalline BiFeO$_3$ via the glycine-nitrate combustion method. *Russ. J. Gen. Chem.*, 2016, **86**(10), P. 2256–2262.

[61] Lomanova N. A., Tomkovich M. V., Danilovich D. P., Osipov A. V., Panchuk V. V., Semenov V. G., Pleshakov I. V., Volkov M. P., Gusarov V. V. Magnetic characteristics of nanocrystalline BiFeO$_3$-based materials prepared by solution combustion synthesis. *Inorg. Mater.*, 2020, **56**(12), P. 1271–1277.

[62] Lomanova N.A., Tomkovich M.V., Sokolov V.V., Ugolkov V.L., Panchuk V.V., Semenov V.G., Pleshakov I.V., Volkov M.P., Gusarov V.V. Thermal and magnetic behavior of BiFeO$_3$ nanoparticles prepared by glycine-nitrate combustion. *Journal of Nanoparticle Research*, 2018, **20**, Art.No 17.

[63] Martinson K.D., Sakhno D.D., Belyak V.E., Kondrashkova I.S. Ni$_{0.4}$Zn$_{0.6}$Fe$_2$O$_4$ nanopowders by solution-combustion synthesis: influence of Red/Ox ratio on their morphology, structure, and magnetic properties. *International Journal of Self-Propagating High-Temperature Synthesis*, 2020, **29**, P. 202–207.

[64] Martinson K.D., Kondrashkova I.S., Popkov V.I. Synthesis of EuFeO3 nanocrystals by glycine-nitrate combustion method. *Russ. J. Appl. Chem.*, 2017, **90**(8), P. 1214–1218.

[65] Dyachenko S.V., Martinson K.D., Cherepkova I.A., Zhernovoi A.I. Particle size, morphology, and properties of transition metal ferrospinels of the MFe$_2$O$_4$ (M = Co, Ni, Zn) type, produced by glycine-nitrate combustion. *Russ. J. Appl. Chem.*, 2016, **89**(4), P. 535–539.

[66] Popkov V.I., Almjasheva O.V. Yttrium orthoferrite YFeO3 nanopowders formation under glycine-nitrate combustion conditions. *Russ. J. Appl. Chem.*, 2014, **87**(2), P. 167–171.

[67] State diagrams of silicate systems. Directory. Issue 2. Metal-oxygen compounds of silicate systems. Ed. N.A.Toropova. Science, Leningrad, 1969, P. 295–298, P. 359–363. (Total 372 p). In Russian.

[68] Shannon R.D. Revised effectiveionic radii and systematic studies of interatomic distances in halides and chalcogenides. *Acta Crystallographica Section A*, 1976, **A32**, P. 751–767.

[69] Gusarov V.V., Semin E.G., Suvorov S.A. Thermodynamics of heterovalent isomorphic mixtures of Be$_{1-1.5x}$Me$_x$O (Me is a 3$d$ element). *Russ. J. Appl. Chem.*, 1983, **56**(9), P. 1956–1958. In Russian

[70] Gusarov V.V., Egorov F.K., Ekimov S.P., Suvorov S.A. Mossbauer study of kinetics of film state formation under the interaction of magnesium and oron-oxides. *Zh. Fiz. Khim.*, 1987, **61**(6), P. 1652–1654. In Russian.

[71] Gusarov V.V., Suvorov S.A. Thickness of 2-demtnsionsl nonautonomous phases in local equilibrium polycrystalline systems based on a single bulk phase. *Russ. J. Appl. Chem.*, 1993, **66**(7), P. 1212–1216.

[72] Gusarov V.V., Popov I.Yu. Flows in Two-dimensional nonautonomous phases in polycrystalline system. *Nuovo Cimento della Societa Italiana di Fisica D*, 1996, **18D**(7), P. 799–805.

[73] Gusarov V.V., Almjasheva O.V. The role of non-autonomous state of matter in the formation of structure and properties of nanomaterials. Chapter 13 in the book *Nanomaterials: properties and promising applications*. Ed A.B. Yaroslavtsev. Scientific World Publishing House, Moscow, 2014, P. 378–403. in Russian

[74] Kirillova S.A., Panchuk V.V., Semenov V.G., Almjasheva O.V. Solid-phase interaction in the ZrO$_2$–Fe$_2$O$_3$ nanocrystalline system. *Nanosystems: Phys., Chem., Math.*, 2018, **9**(6), P. 763–769.

*Information about the authors:*

*Denis D. Averkiev* – Ioffe Institute, St. Petersburg, 194021, Russia; St. Petersburg State Electrotechnical University "LETI", St. Petersburg, 197376, Russia; swnesli2019@gmail.com

*Lyudmila L. Larina* – Solar Photovoltaic Laboratory, Emanuel Institute of Biochemical Physics, Moscow, Russia

*Oleg I. Shevaleevskiy* – Solar Photovoltaic Laboratory, Emanuel Institute of Biochemical Physics, Moscow, Russia; ORCID 0000-0002-8593-3023; shevale2006@yahoo.com

*Oksana V. Almjasheva* – Ioffe Institute, St. Petersburg, 194021, Russia; St. Petersburg State Electrotechnical University "LETI", St. Petersburg, 197376, Russia; ORCID 0000-0002-6132-4178; almjasheva@mail.ru

*Conflict of interest*: the authors declare no conflict of interest.